Finite-difference calculation of the electronic structure of artificial graphene, the 2D hexagonal $Al_wGa_{1-w}As$/GaAs structure with tunable interactions

R. Thirayatorn[a], P. Moontragoon[a,b,*], V. Amornkitbamrung[a,b], S. Meansiri[c], Z. Ikonic[d]

[a] *Department of Physics, Science, Khon Kaen University, Khon Kaen, 40002, Thailand.*
[b] *Integrated Nanotechnology Research Center (INRC), Department of Physics, Science, Khon Kaen University, Khon Kaen, 40002, Thailand.*
[c] *School of Physics, Suranaree University of Technology, Nakhon Ratchasima, 30000, Thailand.*
[d] *School of Electronic and Electrical Engineering, University of Leeds, Leeds, UK.*

Abstract

The energy dispersion relation of two dimensional hexagonal lattice of GaAs quantum wires embedded in $Al_wGa_{1-w}As$ matrix, called artificial graphene, was calculated by the finite difference method with periodic boundary conditions. The validity of the finite difference based code was checked by comparing the bound state energies of various two dimensional systems with appropriate boundary conditions with analytic solutions or the results obtained by COMSOL software, which uses the finite element method, and a very good agreement was found. The energy dispersion relation calculated for artificial graphene structure shows massless Dirac particles, characteristic for real graphene. Therefore, artificial graphene-like structures have properties similar to those of real graphene, and are tailorable by appropriate structure engineering.

Keywords: Artificial graphene, Massless Dirac particle, 2-dimensional energy dispersion relation, band structure engineering

2010 MSC: 82D77, D2D80

1. Introduction

Graphene, a two-dimensional (2D) hexagonal crystalline allotrope with a regular sp2-bonding of carbon, has been attracting the research attention due to a variety of its unique properties, being a strong, light, nearly transparent material, and an excellent conductor of heat and electricity [1, 2]. In particular, it shows an unusual feature in its 2D band structure, with massless Dirac fermions (Dirac cones), showing intrinsically ultrahigh carrier mobilities, since the quasiparticles in it behave like relativistic elementary particles with zero rest mass [3, 4]. Due to these outstanding characteristics, graphene shows extraordinary potential for device applications, like graphene transistors for high-frequency electronics, flexible touch-screen devices, smart windows, batteries,

*Corresponding author
Email address: mpairo@kku.ac.th (P. Moontragoon)

fuel cells, photovoltaic cells and supercapacitors based on graphene, and also has a prospect of replacing metals in the manufacture of aircraft and cars by graphene-plastic composites.

Artificial graphene (a common name for honeycomb lattice materials or structures) provides a tunable platform for investigating massless Dirac quasiparticles, such as their behavior under electric field, magnetic field and band engineering methods [5, 6, 7, 8, 9]. These structures can be fabricated by advanced nanoscale fabrication technology processes, which enable high quality low-dimensional nanoscale patterns that can be precisely controlled. Examples of artificial graphene structures, which were designed and fabricated, are synthetic nanopatterned GaAs heterostructures with ultrahigh-mobility 2D electron gas [10, 11, 12, 13, 14, 15, 16]. These were successfully fabricated by, firstly, using an electron beam nanolithography to produce an array of Nickel disks with the honeycomb geometry, and then by etching away the material outside the disks by inductive-coupled reactive ion etching. Scanning tunneling microscope (STM) was used to pattern the Oxygen and Carbon atoms of CO molecules in a honeycomb pattern. Another example of artificial graphene is based on atoms or molecule manipulated by crystalline-like laser trapping of ultracold atoms. The honeycomb photonic crystal induced by laser irradiation is based on the change of refractive index. In this work, we calculate the bandstructures and energy dispersion relation of an artificial graphene of 2D confined electrons in the $Al_wGa_{1-w}As/GaAs/Al_wGa_{1-w}As$ system.

2. Computational method

In this work the artificial graphene based on quantum wire nanostructure, i.e. the honeycomb structure of $Al_wGa_{1-w}As/GaAs/Al_wGa_{1-w}As$ is considered, with the Al content (w) equal to 0.20. The effective mass method is employed to solve the envelope function Schrödinger equation. The conduction band discontinuity between $Al_wGa_{1-w}As$ and GaAs is taken as $0.79w$ [eV] for $w < 0.41$ [17, 18, 19]. Interdiffusion leads to smoothing of the initially abrupt Al content profile around the interface. In case of cylindrical symmetry the exact analytical solution for the interdiffusion profile exists [20], but is somewhat involved, and the Al profile in the layer plane, $w_{xy}(x, y)$, was here approximated by a simpler expression:

$$w_{xy}(x,y) = \frac{-w}{e^{\beta\left(\sqrt{(x-x_0)^2+(y-y_0)^2}-R_M\right)}+1} + w.$$

Therefore, the two dimensional potential profile in the xy plane, $V(x, y)$, is described by

$$V(x,y) = -\frac{0.79w}{e^{\beta\left(\sqrt{(x-x_0)^2+(y-y_0)^2}-R_M\right)}+1}, \quad (1)$$

where β is the reciprocal diffusion length parameter, (x_0, y_0) is the center of the GaAs wire, and R_M the wire radius, as shown in Fig. 1 (a).

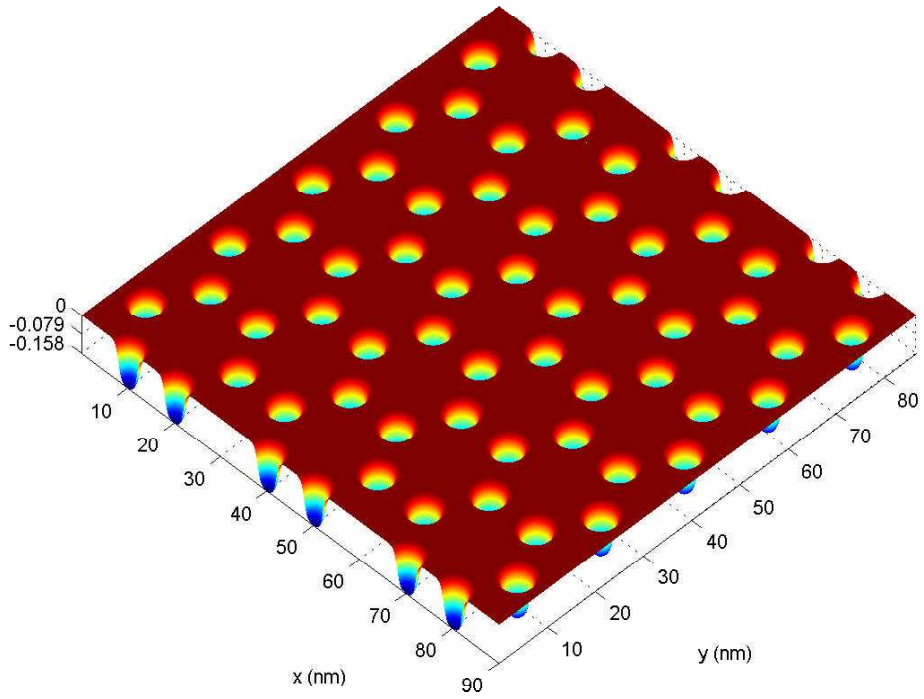

(a)

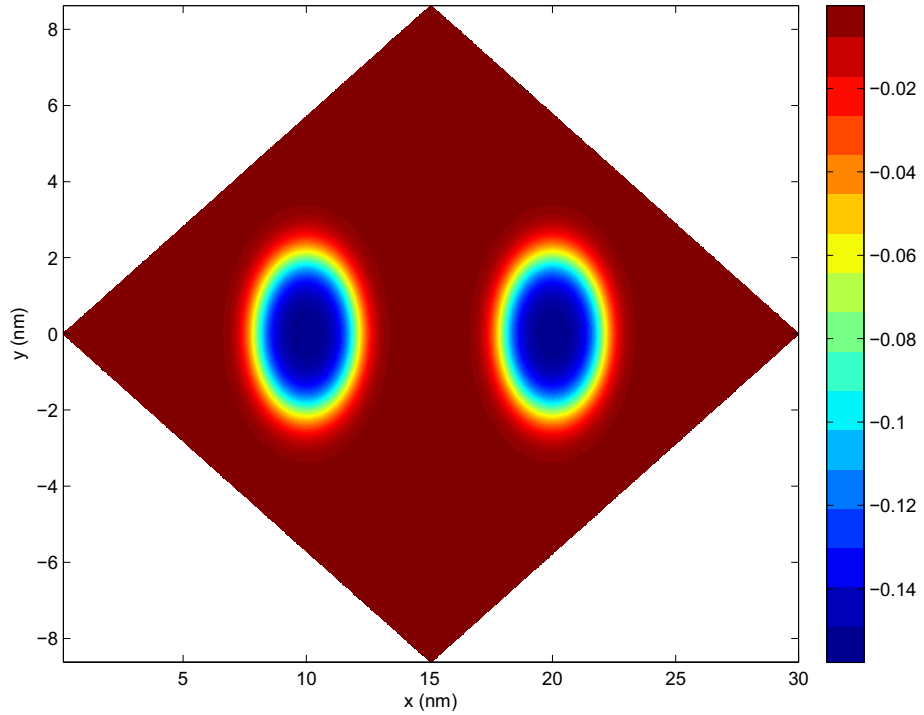

(b)

Figure 1: The potential profile of (a) two dimensional hexagonal lattice $Al_{0.2}Ga_{0.8}As$/ GaAs/ $Al_{0.2}Ga_{0.8}As$, and (b) within a rhomboidal unit cell.

According to the periodicity of this structure, we choose a 2D unit cell as a rhomboid with basis vectors $\mathbf{a}_1 = \frac{L\sqrt{3}}{2}\hat{i} + \frac{L}{2}\hat{j}$ and $\mathbf{a}_2 = \frac{L\sqrt{3}}{2}\hat{i} - \frac{L}{2}\hat{j}$. The lattice constant is $L = \sqrt{3}d_0$, where d_0 is the distance between two neighbouring GaAs wires, as shown in Fig. 1(b). Within the effective mass method, the 2D electron energies and envelope wavefunctions are found from

$$\left\{-\frac{\hbar^2}{2}\left(\nabla\cdot\frac{1}{m^* m_e}\nabla\right)+V\right\}\psi = \epsilon\psi \tag{2}$$

where m_e is the free electron mass, m^* is the position-dependent effective mass, according to the Al content ($m^* = 0.063 + 0.083w$ for w <0.41) [17, 18, 19], and has the similar smooth profile as the potential:

$$\begin{aligned} m^*(x,y) &= 0.063 + 0.083w \\ &- \frac{0.083w}{e^{\beta\left(\sqrt{(x-x_0)^2+(y-y_0)^2}-R_M\right)}+1}, \end{aligned} \tag{3}$$

According to the chosen unit cell, new coordinates (u, v) were introduced to simplify the implementation of periodic boundary conditions: u and v are the coordinates along $\mathbf{a}_1$ and $\mathbf{a}_2$ directions, where $\vec{a}_1$ and $\vec{a}_2$ are the 2D lattice basis vectors, $\vec{a}_1 = \frac{\sqrt{3}L\hat{i}}{2} + \frac{L}{2}\hat{j}$ and $\vec{a}_2 = \frac{\sqrt{3}L\hat{i}}{2} - \frac{L}{2}\hat{j}$. Therefore, u and v take values between 0 and L, and are related to rectangular coordinates x and y as:

$$\begin{bmatrix} u \\ v \end{bmatrix} = \begin{bmatrix} \frac{\sqrt{3}}{3} & 1 \\ \frac{\sqrt{3}}{3} & -1 \end{bmatrix} \begin{bmatrix} x \\ y \end{bmatrix} \tag{4}$$

while (u, v) can be transformed back to (x, y) as

$$\begin{bmatrix} x \\ y \end{bmatrix} = \begin{bmatrix} \frac{\sqrt{3}}{2} & \frac{\sqrt{3}}{2} \\ \frac{1}{2} & -\frac{1}{2} \end{bmatrix} \begin{bmatrix} u \\ v \end{bmatrix} \tag{5}$$

The Schrödinger equation can now be written in the new coordinate system, e.g. in the constant effective mass case the kinetic energy part is

$$\begin{aligned} -\nabla^2\psi &= -\frac{\partial^2\psi}{\partial x^2} - \frac{\partial^2\psi}{\partial y^2} \\ &= -\frac{4}{3}\left\{\frac{\partial^2\psi}{\partial u^2} + \frac{\partial^2\psi}{\partial v^2} - \frac{\partial^2\psi}{\partial u\partial v}\right\} \end{aligned}$$

In order to solve it, the finite difference method has been employed. The terms $\frac{\partial^2\psi}{\partial u^2}$, $\frac{\partial^2\psi}{\partial v^2}$, and $\frac{\partial^2\psi}{\partial u\partial v}$ are written in finite difference form as

$$\left(\frac{\partial^2\psi}{\partial u^2}\right)_{i,j} = \frac{\psi_{i+1,j}-2\psi_{i,j}+\psi_{i-1,j}}{(\Delta u)^2}$$
$$\left(\frac{\partial^2\psi}{\partial v^2}\right)_{i,j} = \frac{\psi_{i,j+1}-2\psi_{i,j}+\psi_{i,j-1}}{(\Delta v)^2}$$
$$\left(\frac{\partial^2\psi}{\partial u\partial v}\right)_{i,j} = \frac{1}{4\Delta u\delta v}\left\{\begin{array}{c}\psi_{i+1,j+1}-\psi_{i+1,j-1}\\-\psi_{i-1,j+1}+\psi_{i-1,j-1}\end{array}\right\}$$

Therefore, the finite-difference form of the 2D Schrödinger equation in the (u, v) coordinates is:

$$-\frac{\hbar^2}{2m}\left\{\begin{array}{c}\frac{\psi_{i-1,j}-2\psi_{i,j}+\psi_{i+1,j}}{(\Delta u)^2}+\frac{\psi_{i,j-1}-2\psi_{i,j}+\psi_{i,j-1}}{(\Delta v)^2}\\-\frac{\psi_{i+1,j+1}-\psi_{i+1,j-1}-\psi_{i-1,j+1}+\psi_{i-1,j-1}}{4\Delta u\delta v}\end{array}\right\}+V_{i,j}\psi_i = \epsilon\psi_{i,j}$$
$$\left\{\begin{array}{c}(-h_u\psi_{i-1,j}+2h_u\psi_{i,j}-h_u\psi_{i+1,j})\\+(-h_v\psi_{i,j-1}+2h_v\psi_{i,j}-h_v\psi_{i,j+1})\\+h_{uv}\psi_{i+1,j+1}-h_{uv}\psi_{i+1,j-1}\\-h_{uv}\psi_{i-1,j+1}+h_{uv}\psi_{i-1,j-1}\end{array}\right\}+V_{i,j}\psi_{i,j} = \epsilon\psi_{i,j}$$
$$\left\{\begin{array}{c}-h_u\psi_{i,j-1}-h_u\psi_{i-1,j}\\+(2h_u+2h_v+V_{i,j})\psi_{i,j}\\-h_u\psi_{i+1,j}-h_u\psi_{i,j+1}\\+h_{uv}\psi_{i+1,j+1}-h_{uv}\psi_{i+1,j-1}\\-h_{uv}\psi_{i-1,j+1}+h_{uv}\psi_{i-1,j-1}\end{array}\right\} = \epsilon\psi_{i,j}$$

where $h_u = \frac{\hbar^2}{2m(\Delta u)^2}$, $h_v = \frac{\hbar^2}{2m(\Delta v)^2}$, $h_{uv} = \frac{\hbar^2}{8m(\Delta u)(\Delta v)}$, and $V_{i,j} = V(u, v)$.

2.1. Validity of the method

In order to check the validity of this method, and of the code developed for it, we have first calculated the bound state energies of three systems: 1) single quantum wire, 2) double quantum wire with rectangular box boundary conditions, and 3) double quantum wire with rhomboidal box boundary conditions.

2.1.1. Single quantum wire

The bound state energies of a 2D infinitely deep square wire with $L_x = L_y = 8$ nm, and of a finite-barrier circular wire with radius of 4 nm and depth of $-0.79w$ eV in a square box, were calculated, assuming a constant effective mass $m^* = 0.063 + \frac{0.083w}{2}$, by using the finite difference method, and were compared against the values obtained by the finite element method or from the analytic solution. The results are shown in Table 1 and indicate the validity of the developed code and the finite difference method.

structure	states	state energy (eV)		
		FDM	FEM	analytic solution
infinite square wire	1	0.1646	0.1646	0.1646
	2	0.4113	0.4115	0.4115
	3	0.4113	0.4115	0.4115
	4	0.6580	0.6585	0.6585
finite circular wire ($R_M = 4$ nm)	1	-0.0731	-0.0743	-0.0758
finite circular wire ($R_M = 5$ nm)	1	-0.0947	-0.0949	-0.0907
	2	-0.0129	-0.0132	-0.0336
	3	-0.0129	-0.0132	-0.0336

Table 1: The state energies of infinitely deep square wire and of a finite-barrier circular wire, calculated by finite difference method (FDM), finite element method (FEM) with COMSOL package [21], and from the analytic solution [22].

2.1.2. Double quantum wires

Using a constant effective mass $m^* = 0.063 + \frac{0.083w}{2}$, we have also calculated the bound state energies of GaAs double cylindrical quantum wires (with a radius of 4, 5, and 6 nm) which were separated by $d_0 = \frac{L\sqrt{3}}{3}$ nm, embedded in $Al_{1-w}Ga_wAs$ matrix of rectangular shape (box) of the size $L_x = 30\sqrt{3}$ nm and $L_y = 30$ nm, as shown in Fig. 2(a), and of rhomboidal shape with $L = 30$ nm, and with the interdiffusion parameter $\beta = 3$, as shown in Fig. 2(b).

In the case of rhomboidal box, the envelope wave functions were gridded along the u and v directions. The Dirichlet boundary conditions are $\psi_{i,0} = \psi_{i,N} = 0$ $(i = 0, 1, 2, 3, .., N)$, and $\psi_{0,j} = \psi_{N,j} = 0$ $(j = 0, 1, 2, 3, .., N)$. Therefore, the wavefunction $\psi_{i,j}$, $i, j = 1, 2, 3, ..., N-1$, can be calculated from $H\psi = \epsilon\psi$ when H is a symmetric matrix of size $(N-1)^2 \times (N-1)^2$, and the content of upper triangle of this matrix is:

$$H = \begin{bmatrix} A_1 & B & 0 & 0 & \cdots & 0 & 0 & 0 \\ B^T & A_2 & B & 0 & \cdots & 0 & 0 & 0 \\ 0 & B^T & A_3 & B & \cdots & 0 & 0 & 0 \\ \vdots & \vdots & \vdots & \vdots & \ddots & \vdots & \vdots & \vdots \\ 0 & 0 & 0 & 0 & B^T & A_{N-3} & B & 0 \\ 0 & 0 & 0 & 0 & 0 & B^T & A_{N-2} & B \\ 0 & 0 & 0 & 0 & 0 & 0 & B^T & A_{N-1} \end{bmatrix} \quad (6)$$

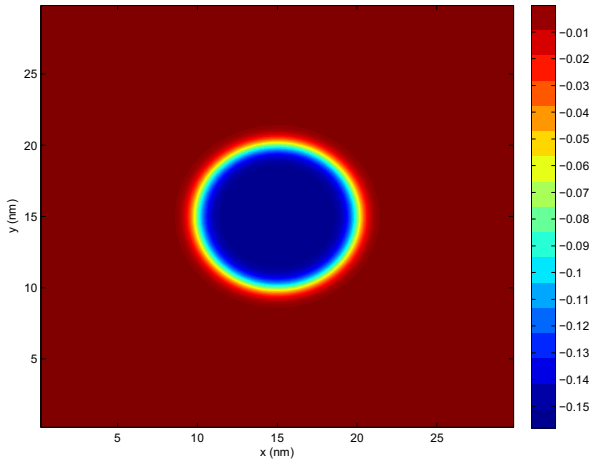

(a)

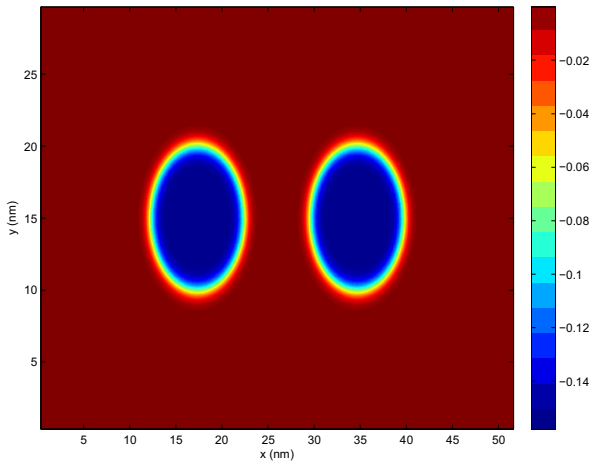

(b)

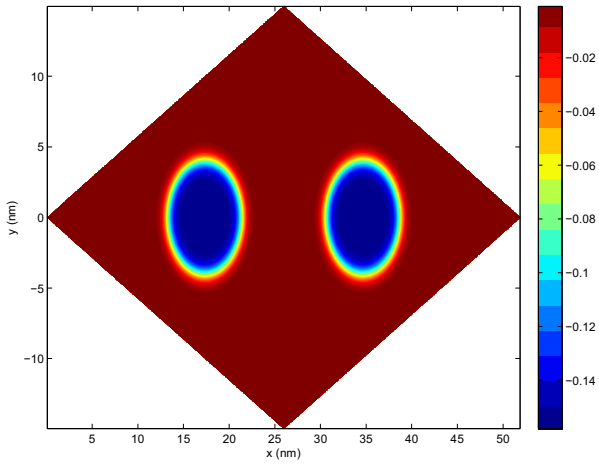

(c)

Figure 2: The potential profile of (a) single and double cylindrical $Al_{0.2}Ga_{0.8}As$/ GaAs/ $Al_{0.2}Ga_{0.8}As$ quantum wires, with (b) rectangular boundary conditions, and (c) with rhomboidal boundary conditions.

where the matrix A_j and B are

$$A_j = \begin{bmatrix} c_{1,j} & -h_v & 0 & 0 & \cdots & 0 & 0 & 0 \\ -h_v & c_{2,j} & -h_v & 0 & \cdots & 0 & 0 & 0 \\ 0 & -h_v & c_{3,j} & -h_v & \cdots & 0 & 0 & 0 \\ \vdots & \vdots & \vdots & \vdots & \ddots & \vdots & \vdots & \vdots \\ 0 & 0 & 0 & 0 & -h_v & c_{N-3,j} & -h_v & 0 \\ 0 & 0 & 0 & 0 & 0 & -h_v & c_{N-2,j} & -h_v \\ 0 & 0 & 0 & 0 & 0 & 0 & -h_v & c_{N-1,j} \end{bmatrix} \tag{7}$$

and

$$B = \begin{bmatrix} h_u & h_{uv} & 0 & 0 & \cdots & 0 & 0 & 0 \\ -h_{uv} & h_u & h_{uv} & 0 & \cdots & 0 & 0 & 0 \\ 0 & -h_{uv} & h_u & h_{uv} & \cdots & 0 & 0 & 0 \\ \vdots & \vdots & \vdots & \vdots & \ddots & \vdots & \vdots & \vdots \\ 0 & 0 & 0 & 0 & -h_{uv} & h_u & h_{uv} & 0 \\ 0 & 0 & 0 & 0 & 0 & -h_{uv} & h_u & h_{uv} \\ 0 & 0 & 0 & 0 & 0 & 0 & -h_{uv} & h_u \end{bmatrix} \tag{8}$$

where the sizes of matrices A_j and B are $(N-1) \times (N-1)$, and $c_{i,j} = 2h_u + 2h_v + V_{i,j}$. The eigenvalues and eigenvectors of H are the state energies and the envelope wave functions, the latter given in the (u, v) coordinate system, i.e. $\psi_{i,j} = \{\ \psi_{1,1}, \psi_{1,2}, \psi_{1,3}, ..., \psi_{1,N-1}, \psi_{2,1}, \psi_{2,2}, \psi_{2,3}, ..., \psi_{2,N-1}, ..., \psi_{N-1,1}, \psi_{N-1,2}, \psi_{N-1,3}, ..., \psi_{N-1,N-1}\ \}$.

In case of rectangular box, the envelope wave functions were grided along x and y directions, and the parameters were transformed as $h_u \Rightarrow h_y = \frac{\hbar^2}{2m(\Delta y)^2}$, $h_v \Rightarrow h_x = \frac{\hbar^2}{2m(\Delta x)^2}$, $h_{uv} \Rightarrow h_x = 0$, and $V_{i,j} = V(x, y)$. The results were compared against the state energies and wavefunctions obtained from the COMSOL software [21], which uses the finite element method, Fig. 3 (a), (b) and Table 2. The two methods are in good agreement, particularly for low-energy states, and the described finite difference method was further employed for this structure.

3. Results

3.1. 2D energy band structure

The periodic potential $V(\mathbf{r})$ with period of L in both u and v directions, shown in Fig. 1 (b), has the property:

$$V(\mathbf{r}) = V(\mathbf{r} + \mathbf{R}) \tag{9}$$

where $\mathbf{R}$ is any translation vector for this unit cell. The wave functions then must satisfy the

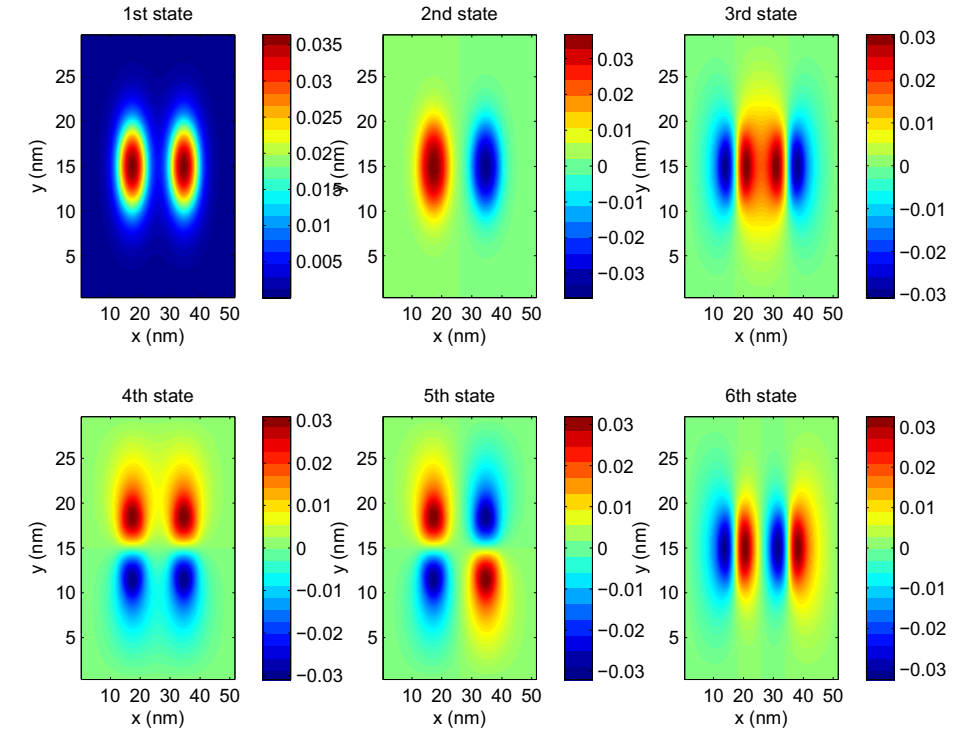

(a)

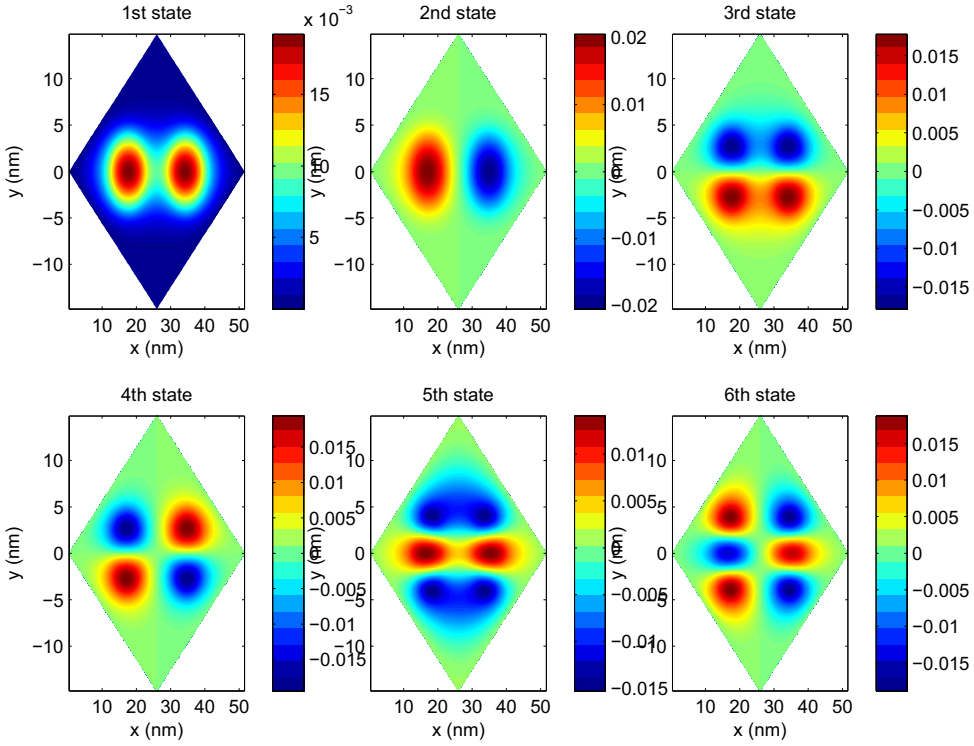

(b)

Figure 3: The envelope wave functions of double GaAs cylindrical quantum wires embedded in $Al_{0.2}Ga_{0.8}As$ matrix, with (a) rectangular boundary conditions, and (b) rhomboidal boundary conditions. calculated by the finite difference method.

R_M (nm)	states	state energy (eV)			
		rhomboid		rectangular	
		FDM	FEM	FDM	FEM
4	1	-0.0648	-0.0713	-0.0721	-0.0720
	2	-0.0545	-0.0705	-0.0714	-0.0713
	3	-0.0095	0.0139	-0.0088	0.0088
	4	0.0053	0.0236	0.0113	0.0114
	5	0.0331	0.0302	0.0153	0.0154
	6	0.0520	0.0302	0.0167	0.0167
5	1	-0.0856	-0.0924	-0.0932	-0.0931
	2	-0.0751	-0.0916	-0.0925	-0.0924
	3	-0.0388	-0.0121	-0.0154	-0.0153
	4	-0.0267	-0.0055	-0.0128	-0.0127
	5	0.0131	-0.0031	-0.0110	-0.0108
	6	0.0327	-0.0031	-0.0079	-0.0077
6	1	-0.1015	-0.1070	-0.1081	-0.1083
	2	-0.0895	-0.1059	-0.1071	-0.1072
	3	-0.0622	-0.0394	-0.0422	-0.0420
	4	-0.0505	-0.0333	-0.0395	-0.0390
	5	-0.0150	-0.0317	-0.0382	-0.0380
	6	-0.0001	-0.0317	-0.0351	-0.0350

Table 2: The state energies of double cylindrical quantum wire with rhomboidal and rectangular box boundary conditions, calculated by finite difference method (FDM) and finite element method (FEM) with COMSOL package.

Bloch conditions, i.e. the wave functions can be written as the product of a periodic function $u(\vec{r})$ and $e^{i\vec{k}\cdot\vec{r}}$

$$\psi_{\vec{k}}(\vec{r}) = u_{\vec{k}}(\vec{r})e^{i\vec{k}\cdot\vec{r}}, \tag{10}$$

and where the periodicity of $u_{\vec{k}}(\vec{r})$ is the same as that of the potential. Therefore, the particle wave functions in each period differ only by the phase factor $e^{i\vec{k}\cdot\vec{R}}$, i.e.

$$\psi_{\vec{k}}(\vec{r}) = \psi_{\vec{k}}(\vec{r}+\vec{R})e^{-i\vec{k}\cdot\vec{R}}, \tag{11}$$

where $\mathbf{k}$ is the wave vector (crystal momentum). The Hamiltonian matrix H is a hermitian matrix of size of $N^2 \times N^2$, where N is the number of grid points along u and v directions, and its

matrix elements are

$$H = \begin{bmatrix} A_1 & B & 0 & 0 & \cdots & 0 & 0 & C \\ B^\dagger & A_2 & B & 0 & \cdots & 0 & 0 & 0 \\ 0 & B^\dagger & A_3 & B & \cdots & 0 & 0 & 0 \\ \vdots & \vdots & \vdots & \vdots & \ddots & \vdots & \vdots & \vdots \\ 0 & 0 & 0 & 0 & B^\dagger & A_{N-2} & B & 0 \\ 0 & 0 & 0 & 0 & 0 & B^\dagger & A_{N-1} & B \\ C^\dagger & 0 & 0 & 0 & 0 & 0 & B^\dagger & A_N \end{bmatrix} \tag{12}$$

where the matrices A_j and B are

$$A_j = \begin{bmatrix} c_{1,j} & -h_v & 0 & 0 & \cdots & 0 & 0 & -h_v f_v \\ -h_v & c_{2,j} & -h_v & 0 & \cdots & 0 & 0 & 0 \\ 0 & -h_v & c_{3,j} & -h_v & \cdots & 0 & 0 & 0 \\ \vdots & \vdots & \vdots & \vdots & \ddots & \vdots & \vdots & \vdots \\ 0 & 0 & 0 & 0 & -h_v & c_{N-2,j} & -h_v & 0 \\ 0 & 0 & 0 & 0 & 0 & -h_v & c_{N-1,j} & -h_v \\ -h_v f_v^* & 0 & 0 & 0 & 0 & 0 & -h_v & c_{N,j} \end{bmatrix} \tag{13}$$

and

$$B = \begin{bmatrix} h_u & h_{uv} & 0 & 0 & \cdots & 0 & 0 & -h_{uv} f_v \\ -h_{uv} & h_u & h_{uv} & 0 & \cdots & 0 & 0 & 0 \\ 0 & -h_{uv} & h_u & h_{uv} & \cdots & 0 & 0 & 0 \\ \vdots & \vdots & \vdots & \vdots & \ddots & \vdots & \vdots & \vdots \\ 0 & 0 & 0 & 0 & -h_{uv} & h_u & h_{uv} & 0 \\ 0 & 0 & 0 & 0 & 0 & -h_{uv} & h_u & h_{uv} \\ h_{uv} f_v^* & 0 & 0 & 0 & 0 & 0 & -h_{uv} & h_u \end{bmatrix} \tag{14}$$

where $C = f_u B$, $f_u = e^{ik_u L}$, $f_v = e^{ik_v L}$, and the sizes of matrices B and C are $N \times N$.

The eigenvalues and eigenvectors of the Hamiltonian matrix are the state energies and wavefunctions of band n and wave vector $\vec{k} = (k_u, k_v) = \left(\{-\frac{\vec{b}_1}{2}, ..., \frac{\vec{b}_1}{2}\}, \{-\frac{\vec{b}_2}{2}, ..., \frac{\vec{b}_2}{2}\}\right)$, as shown in Fig. 4 and 5. In order to check the validity of this method for the periodic boundary conditions, the results were compared with those obtained with the, more conventional for periodic structures, plane wave basis functions expansion (formally a linear variational method) as was employed in [9]. In the plane wave method the wavefunction is written as

$$\psi_{n,\vec{k}}(\vec{r}) = \sum_{\vec{G}} c_{\vec{G}} \frac{1}{\sqrt{\Omega}} e^{i(\vec{k}+\vec{G})\cdot\vec{r}}, \tag{15}$$

where $c_{\vec{G}}$ are the plane wave amplitude coefficients. The Hamiltonian matrix, $H_{\vec{G},\vec{G}'}$, will be

$$H_{\vec{G},\vec{G}'} = \frac{\hbar^2}{2m}(\vec{k}+\vec{G})^2\delta_{\vec{G},\vec{G}'} + V(\vec{G}-\vec{G}'), \tag{16}$$

where $\vec{G}$ are the reciprocal lattice vectors and $V(\vec{G}-\vec{G}')$ is the Fourier transform of the potential $V(\vec{r})$, calculated as the 2D Fourier transform of the honeycomb potential (shown in Fig. 1, and with Eq. (1)), with the rhomboidal unit cell defining the structure periodicity. The eigenvalues of the Hamiltonian matrix for any particular wave vector $\vec{k}$ are the band energies.

Examples of results obtained by the finite difference method and the plane wave method are shown in Fig. 5. The agreement between the two is generally very good. In case of sharp boundaries (almost no interdiffusion, $\beta = 100$), the number of space grid points in the finite difference method, and the number of waves in the plane wave method, required for well converged results, are both larger than the what is needed in case of large interdiffusion. The convergence of the finite difference method improves (requiring a smaller number of grid points) for sharp boundaries, while the convergence of the plane wave method improves for large interdiffusion. However, the overall computation time is still smaller with the finite difference than with the plane wave method for any realistic case we have tested (having 8, 16, 32 and 64 grid points per direction, or a total of 8^2, 16^2, 32^2 and 64^2 plane waves), regardless of the level of interdiffusion.

3.2. Effect of position-dependent effective mass

In the previous subsection the two-dimensional band structure of artificial graphene was calculated, but the effective mass was assumed constant. In order to include the effect position-dependent effective mass, we have simplified the problem by changing the unit cell from rhomboidal to rectangular, with basis vectors $\vec{a}_1 = L_x\hat{i} = 3d_0\hat{i}$ and $\vec{a}_2 = L_y\hat{j} = \sqrt{3}d_0\hat{j}$, as shown in Fig. 6.

The 2D Schrödinger equation

$$-\frac{\hbar^2}{2}\left\{\frac{\partial}{\partial x}\left(\frac{1}{m^*(x,y)}\frac{\partial}{\partial x}\psi\right) + \frac{\partial}{\partial y}\left(\frac{1}{m^*(x,y)}\frac{\partial}{\partial y}\psi\right)\right\} + V(x,y)\psi = \epsilon\psi,$$

was written in finite difference form as [23]

$$\left\{\begin{array}{l} +h_x\left(-\frac{\psi_{i-1,j}}{m_{i-\frac{1}{2},j}} + \frac{\psi_{i,j}}{m_{i-\frac{1}{2},j}} + \frac{\psi_{i,j}}{m_{i+\frac{1}{2},j}} - \frac{\psi_{i+1,j}}{m_{i+\frac{1}{2},j}}\right) \\ +h_y\left(-\frac{\psi_{i,j-1}}{m_{i,j-\frac{1}{2}}} + \frac{\psi_{i,j}}{m_{i,j-\frac{1}{2}}} + \frac{\psi_{i,j}}{m_{i,j+\frac{1}{2}}} - \frac{\psi_{i,j+1}}{m_{i,j+\frac{1}{2}}}\right) \end{array}\right\} + V_{i,j}\psi_{i,j} = \epsilon\psi_{i,j},$$

or

$$\left\{\begin{array}{c} \left(-\frac{h_y\psi_{i,j-1}}{m_{i,j-\frac{1}{2}}}\right) \\ -\frac{h_x\psi_{i-1,j}}{m_{i-\frac{1}{2},j}} + \left(+\frac{h_x}{m_{i-\frac{1}{2},j}} + \frac{h_x}{m_{i+\frac{1}{2},j}} + \frac{h_y}{m_{i,j-\frac{1}{2}}} + \frac{h_y}{m_{i,j+\frac{1}{2}}} + V_{i,j}\right)\psi_{i,j} - \frac{h_x\psi_{i+1,j}}{m_{i+\frac{1}{2},j}} \\ \left(-\frac{h_y\psi_{i,j+1}}{m_{i,j+\frac{1}{2}}}\right) \end{array}\right\} = \epsilon\psi_{i,j},$$

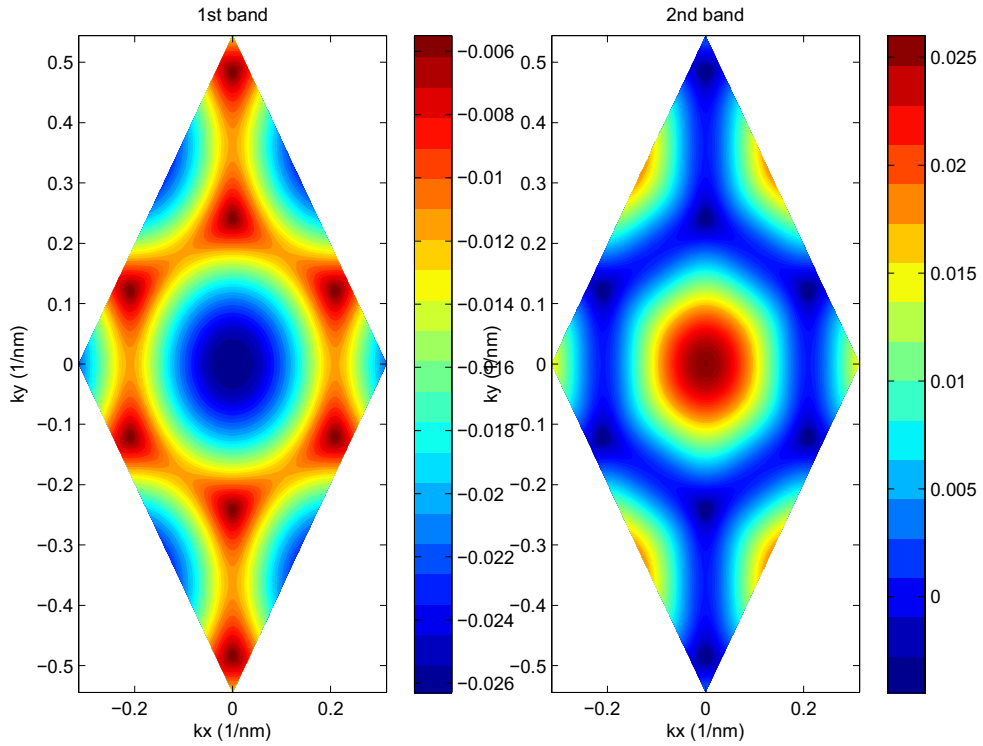

(a)

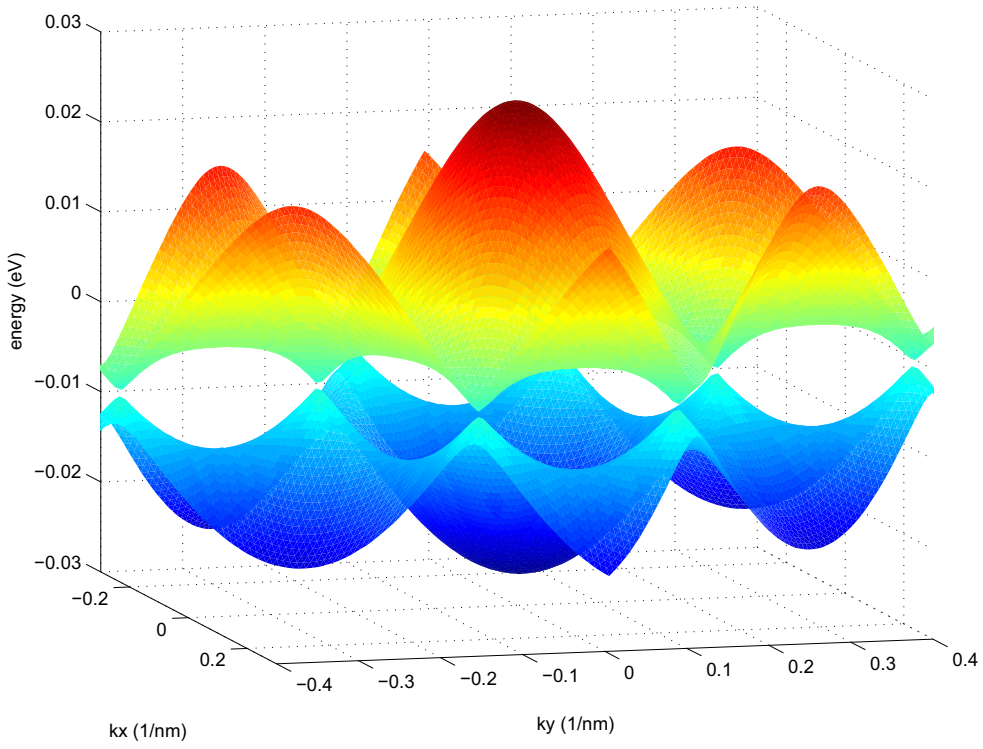

(b)

Figure 4: The energy dispersion for a rhomboidal unit cell artificial graphene $Al_{0.2}Ga_{0.8}As$/ GaAs/ $Al_{0.2}Ga_{0.8}As$ structure.

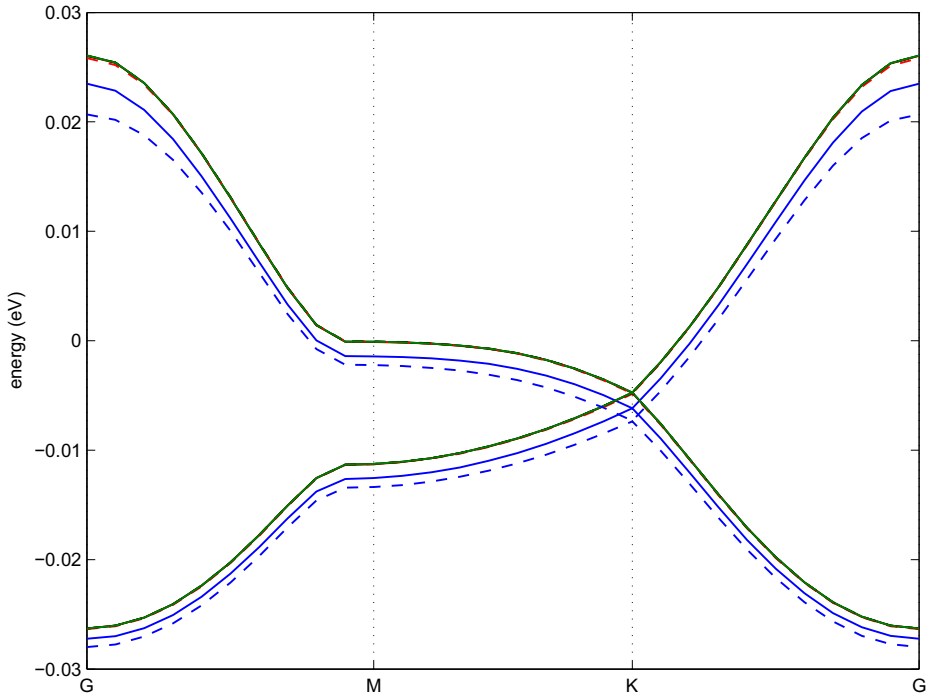

(a)

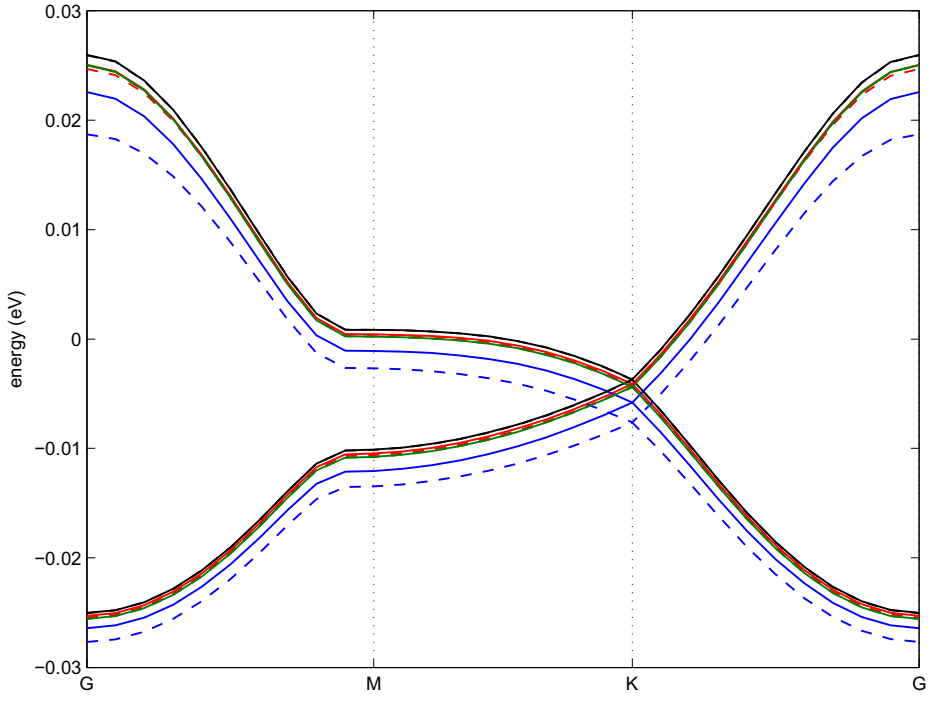

(b)

Figure 5: The band structure of rhomboidal unit cell artificial graphene $Al_{0.2}Ga_{0.8}As$/ GaAs/ $Al_{0.2}Ga_{0.8}As$ along special high-symmetry directions in the two-dimensional hexagonal Brillouin zone (G=(0,0), M=$(1/\sqrt{3},0)2\pi/a$, K=$(0,2/3)2\pi/a$), calculated by finite difference (solid lines) and plane wave method (dashed lines) in the case of (a) large interdiffusion, $\beta = 3$ and (b) small interdiffusion, $\beta = 100$. The blue, black, red and green lines correspond to the number of grid points of 8, 16, 32 and 64, respectively, in each direction, or to the number of plane waves of 8^2, 16^2, 32^2 and 64^2. The energy is measured from the conduction band edge of the matrix material, because the potential, Eq. (1), was defined in this manner.

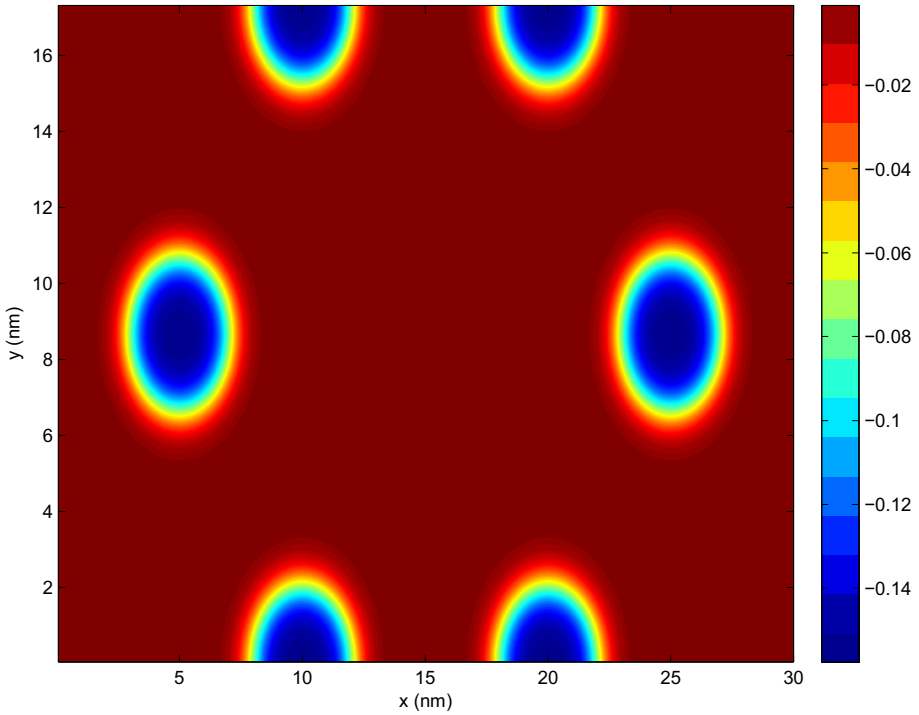

Figure 6: The smoothed potential profile in a rectangular unit cell of artificial graphene $Al_{0.2}Ga_{0.8}As$/ GaAs/ $Al_{0.2}Ga_{0.8}As$.

where the effective mass $m^*(x,y) = m(x,y)m_e$, $h_x = \frac{\hbar^2}{2m_e(\Delta x)^2}$, and $h_y = \frac{\hbar^2}{2m_e(\Delta y)^2}$, while N_x and N_y are the number of grid points in x and y directions, respectively. The Hamiltonian matrix, H, is a square Hermitian matrix of size $N_xN_y \times N_xN_y$, and the upper triangle matrix elements are

$$H = \begin{bmatrix} A_1 & B_1 & 0 & 0 & \cdots & 0 & 0 & C \\ & A_2 & B_2 & 0 & 0 & \cdots & 0 & 0 \\ & & A_3 & B_3 & 0 & 0 & \cdots & 0 \\ & & & & \ddots & & & \\ & & & & A_{N_y-3} & B_{N_y-3} & 0 & 0 \\ & & & & & A_{N_y-2} & B_{N_y-2} & 0 \\ & & & & & & A_{N_y-1} & B_{N_y-1} \\ & & & & & & & A_{N_y} \end{bmatrix} \tag{17}$$

where

$$A_j = \begin{bmatrix} c_{1,j} & r_{1,j} & 0 & 0 & \cdots & 0 & 0 & l_{1,j}f_x \\ & c_{2,j} & r_{2,j} & 0 & 0 & \cdots & 0 & 0 \\ & & c_{3,j} & r_{3,j} & 0 & 0 & \cdots & 0 \\ & & & & \ddots & & & \\ & & & & c_{N_x-3,j} & r_{N_x-3,j} & 0 & 0 \\ & & & & & c_{N_x-2,j} & r_{N_x-2,j} & 0 \\ & & & & & & c_{N_x-1,j} & r_{N_x-1,j} \\ & & & & & & & c_{N_x,j} \end{bmatrix} \quad (18)$$

$$B_j = \begin{bmatrix} d_{1,j} & 0 & 0 & \cdots & 0 & 0 & 0 & 0 \\ & d_{2,j} & 0 & 0 & \cdots & 0 & 0 & 0 \\ & & d_{3,j} & 0 & 0 & \cdots & 0 & 0 \\ & & & & \ddots & & & \\ & & & & d_{N_x-3,j} & 0 & 0 & 0 \\ & & & & & d_{N_x-2,j} & 0 & 0 \\ & & & & & & d_{N_x-1,j} & 0 \\ & & & & & & & d_{N_x,j} \end{bmatrix} \quad (19)$$

$$C = f_y \begin{bmatrix} u_{1,j} & 0 & 0 & \cdots & 0 & 0 & 0 & 0 \\ & u_{2,j} & 0 & 0 & \cdots & 0 & 0 & 0 \\ & & u_{3,j} & 0 & 0 & \cdots & 0 & 0 \\ & & & & \ddots & & & \\ & & & & u_{N_x-3,j} & 0 & 0 & 0 \\ & & & & & u_{N_x-2,j} & 0 & 0 \\ & & & & & & u_{N_x-1,j} & 0 \\ & & & & & & & u_{N_x,j} \end{bmatrix} \quad (20)$$

with

$$c_{i,j} = \left(+ \frac{h_x}{m_{i-\frac{1}{2},j}} + \frac{h_x}{m_{i+\frac{1}{2},j}} + \frac{h_y}{m_{i,j-\frac{1}{2}}} + \frac{h_y}{m_{i,j+\frac{1}{2}}} + V_{i,j} \right)$$

$$u_{i,j} = -\frac{h_y}{m_{i,j-\frac{1}{2}}}, \quad l_{i,j} = -\frac{h_x}{m_{i-\frac{1}{2},j}}, \quad r_{i,j} = -\frac{h_x}{m_{i+\frac{1}{2},j}}, \quad d_{i,j} = -\frac{h_y}{m_{i,j+\frac{1}{2}}}$$

and $f_y = e^{ik_y L_y}$, $f_x = e^{ik_x L_x}$. The sizes of matrices B_j, $B_j^\dagger$, C, and $C^\dagger$ are $N_x \times N_x$. The eigenvalues and eigenvectors of the Hamiltonian matrix are the state energies and wavefunction of band n for wave vector $\vec{k} = (k_x, k_y) = \left(\{-\frac{\pi}{L_x}, ..., \frac{\pi}{L_x}\}, \{-\frac{\pi}{L_y}, ..., \frac{\pi}{L_y}\} \right)$.

An example calculation of this type, shown in Fig. 7(a), shows the influence of the position-dependent effective mass on the band structure of rectangular unit cell artificial graphene $Al_{1-w}Ga_wAs/$

$Al_{1-z}Ga_zAs$/ $Al_{1-w}Ga_wAs$. There are only quantitative differences, compared to the constant effective mass case (and these will depend on this constant mass value taken), but the band structure does show Dirac points in the position-dependent mass as well.

To illustrate the band engineering possibilities in artificial graphene, Fig. 8(b,c) shows the band structures obtained for different values of wire radii R_M and cell sizes d_0 (distance between two neighbouring GaAs wires). Yet another way of band structure tuning, offered by artificial graphene, is by band gap opening at the Dirac points. This is achievable by breaking the symmetry, i.e. the equivalence of sites A and B in the hexagonal lattice, via changing the Al content only in the wires at site A sublattice of the honeycomb lattice structure, as illustrated in Fig. 8(d).

4. Conclusions

The energy dispersion relation for artificial graphene, the two dimensional hexagonal lattice of $Al_wGa_{1-w}As$/ GaAs/ $Al_wGa_{1-w}As$, was calculated by finite difference method. The effect of aluminium interdiffusion between GaAs quantum wires and the $Al_wGa_{1-w}As$ matrix was taken into account by smoothing the potential and effective mass profiles between the two layers. The validity of the finite difference method and the developed code was checked by comparing the bound state energies with analytic solutions in the case of single quantum wire or, in cases of double quantum wires with constant or discontinuous effective mass, with the results obtained from the finite element based COMSOL software. The energy dispersion relation of the artificial graphene shows massless Dirac particles and offers band structure engineering possibilities.

5. Acknowledgment

Funding for this work is provided by Thailand Research Fund (TRF), Integrated Nanotechnology Research Center (INRC), Khon Kaen University (KKU) and the Institute of the Promotion of Teaching Science and Technology (IPST), the Nanotechnology Center (NANOTEC), NSTDA, Ministry of Science and Technology, Thailand, through its program of Center of Excellence Network.

References

[1] K. S. Novoselov, V. I. Fal'ko, L. Colombo, P. R. Gellert, M. G. Schwab, and K. Kim, "A roadmap for graphene", *Nature* 490, 192-200 (2012).

[2] L. Britnell, R. V. Gorbachev, A. K. Geim, L. A. Ponomarenko, A. Mishchenko, M. T. Greenaway, T. M. Fromhold, K. S. Novoselov, and L. Eaves, "Resonant tunnelling and negative differential conductance in graphene transistors", *Nature Communications* 4, 1794 (2013).

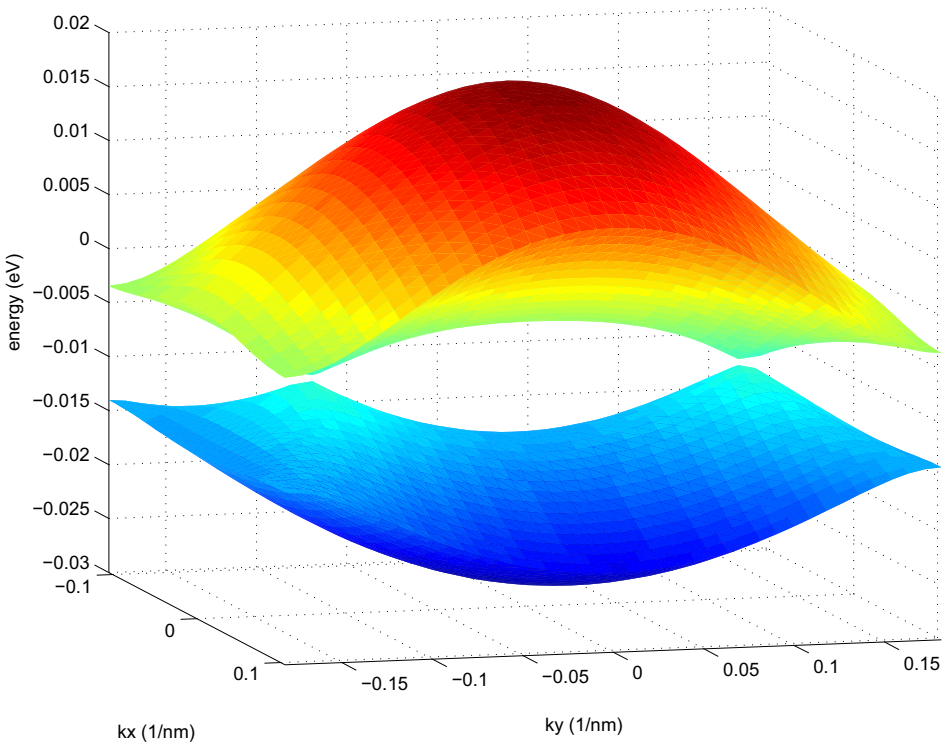

(a)

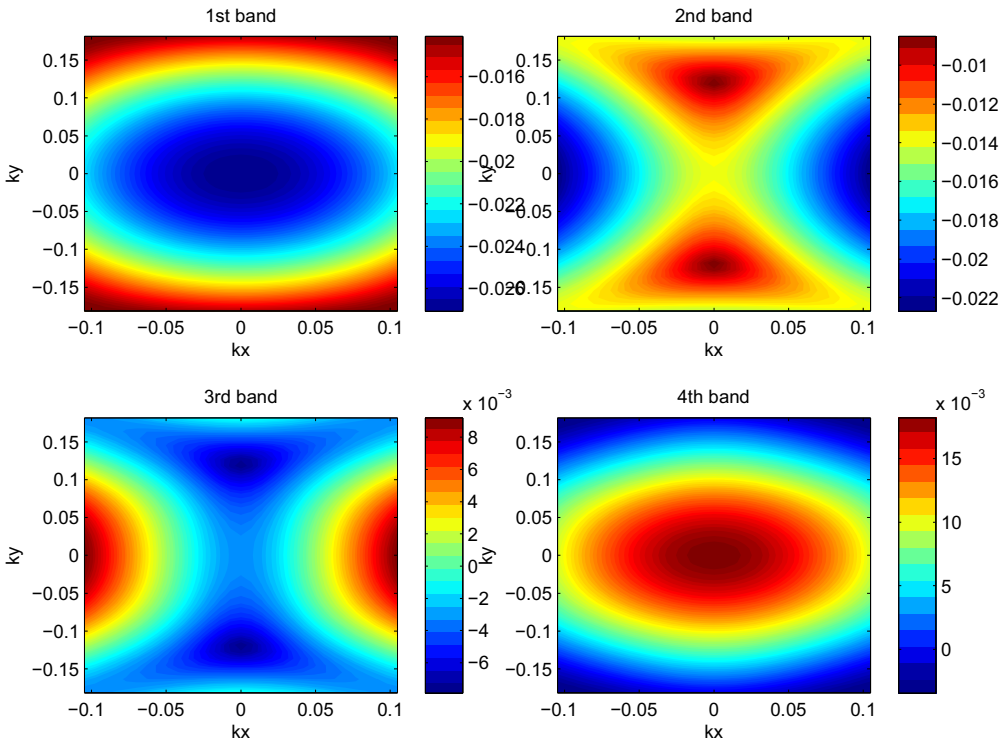

(b)

Figure 7: The energy dispersion for rectangular unit cell artificial graphene $Al_{0.8}Ga_{0.2}As$/ GaAs/ $Al_{0.8}Ga_{0.2}As$.

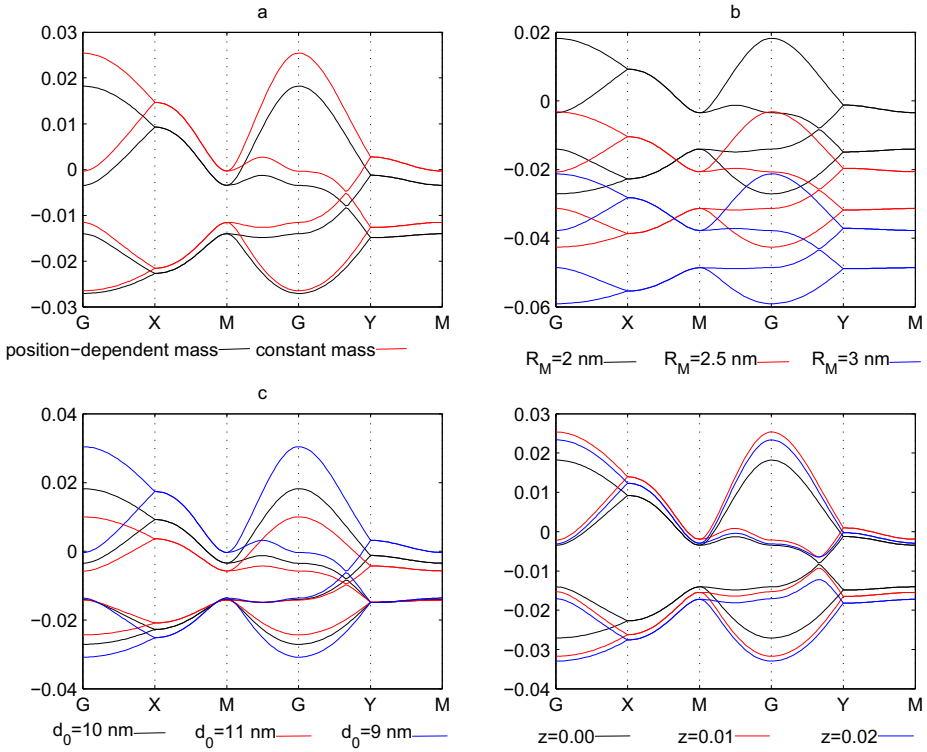

Figure 8: (a) The influence of the position-dependent effective mass on the band structure along special high-symmetry directions in the two-dimensional rectangular Brillouin zone (G=(0,0), M=(0.5,0.5)2π/a, X=(0.5,0)2π/a, Y=(0,0.5)2π/a) of rectangular unit cell artificial graphene $Al_{1-w}Ga_wAs$/ $Al_{1-z}Ga_zAs$/ $Al_{1-w}Ga_wAs$, and the band structure tunability achievable by varying: (b) the wire radius (R_M), (c) the cell size (d_0), and (d) the Al content (z) in wires only at site A sublattice of the honeycomb lattice structure. The energy is measured from the conduction band edge of the matrix material, because the potential, Eq. (1), was defined in this manner.

[3] K. S. Novoselov, A. K. Geim, S. V. Morozov, D. Jiang, M. I. Katsnelson, I. V. Grigorieva, S. V. Dubonos, and A. A. Firsov, "Two-dimensional gas of massless Dirac fermions in graphene", *Nature* 438, 197-200 (2005).

[4] Y. Zhang,Y. W. Tan, H. L. Stormer, and P. Kim, "Experimental observation of the quantum Hall effect and Berry's phase in graphene". *Nature* 438, 201-204 (2005).

[5] Yuan Jian-Hui, Zhang Jian-Jun, Zeng Qi-Jun, Zhang Jun-Pei, and Cheng Ze, "Confined State and Electronic Transport in an Artificial Graphene-Based Tunnel Junction", *Commun. Theor. Phys.* 56, 1135 (2011).

[6] L. Nadvornik, M. Orlita, N. A. Goncharuk, L. Smrcka, V. Novak, V. Jurka, K. Hruska, Z. Vyborny, Z. R. Wasilewski, M. Potemski and K. Vyborny. "From laterally modulated two-dimensional electron gas towards artificial graphene", *New J. Phys.* 14 053002 (2012).

[7] T. Uehlinger, G. Jotzu, M. Messer, D. Greif, W. Hofstetter, U. Bissbort, and T Esslinger, "Artificial Graphene with Tunable Interactions", *Physical Review Letters* 111, 185307 (2013).

[8] E. Rasanen, C. A. Rozzi, S. Pittalis, and G. Vignale, "Electron-Electron Interactions in Artificial Graphene", *Physical Review Letters* 108, 246803 (2012).

[9] M Gibertini, A Singha, V Pellegrini, M Polini, G Vignale, and A Pinczuk "Engineering artificial graphene in a two-dimensional electron gas", *Physical Review B* 79, 241406(R) (2009).

[10] M. Polini, F. Guinea, M. Lewenstein, H. C. Manoharan and V. Pellegrini, "Artificial honeycomb lattices for electrons, atoms and photons", *Nature Nanotechnology* 8, 625633 (2013).

[11] L. Tarruell, D. Greif, T. Uehlinger, G. Jotzu, and T. Esslinger, "Creating, moving and merging Dirac points with a Fermi gas in a tunable honeycomb lattice", *Nature* 483, 302305 (2012).

[12] K. K. Gomes, Warren Mar, W. Ko, F. Guinea, and H. C. Manoharan, "Designer Dirac fermions and topological phases in molecular graphene", *Nature* 483, 306310 (2012).

[13] J. Simon, and M. Greiner, "Condensed-matter physics: A duo of graphene mimics", *Nature* 483, 282284 (2012).

[14] J. Peng and S. S. Li, "Band structures of graphene hexagonal lattice semiconductor quantum dots", *Applied Physics Letters* 97, 242105 (2010).

[15] L. A. Ponomarenko, R. V. Gorbachev, G. L. Yu, D. C. Elias, R. Jalil, A. A. Patel, A. Mishchenko, A. S. Mayorov, C. R.Woods, J. R.Wallbank, M. Mucha-Kruczynski, B. A. Piot, M. Potemski, I. V. Grigorieva, K. S. Novoselov, F. Guinea, V. I. Falko, and A. K. Geim, "Cloning of Dirac fermions in graphene superlattices", *Nature* 497, 594597 (2013).

[16] E. S. Reich, "Graphene knock-offs probe ultrafast electronics", *Nature* 497, 422-423 (2013).

[17] S. C. Jain, and D. J. Roulston, *Solid State Electron*, 34, no.5, pp.453-465 (1991).

[18] A. K. Saxena, *J. Phys. C.*, 13, no.23, pp. 4323-4334 (1980).

[19] M. Levinshtein, "Handbook Series on Semiconductor Parameters, Volume 2", World Scientific, 1996.

[20] V. L. Aziz-Aghchegala, V. N. Mughnetsyan, and A. A. Kirakosyan, "Effect of interdiffusion on electronic states in one-layer quantum ring superlattice", *Physica E*, 64, 51-56 (2014).

[21] COMSOL Inc., 2013. COMSOL Multiphysics Users Guide, 2013. Version 4.3b, COMSOL AB, Stockholm, Sweden.

[22] Kirkman, T. (2015, January 21). "Finite Round Square Well Bound States". Retrieved from http://www.physics.csbsju.edu/QM/square.09.html

[23] P. Harrison, "Quantum Wells, Wires and Dots: Theoretical and Computational Physics of Semiconductor Nanostructures", Wiley, Third Edition, 2009.